Materials Today Communications 50 (2026) 114599

Contents lists available at ScienceDirect

Materials Today Communications

journal homepage: www.elsevier.com/locate/mtcomm

Comparative study of extrapolation and direct methods for FLD prediction in friction stir welded aluminum sheets

Mohamed Lamine Kheroufi [a,b], A. Amirat [c], W. Ghennai [b,d], Sandra Zimmer-Chevret [e], D. Belfenneche [b], R. Yekhlef [b], S. Alomairy [f], M.A. Ghebouli [g,h], Aseel Smerat [i,j], M. Fatmi [g,*]

[a] Laboratory of metal materials forming (LMF2M), Faculty of Technology, Badji Mokhtar University, Annaba, Algeria
[b] Research Center in Industrial Technologies CRTI, P.O. Box 64, Cheraga, Algiers 16014, Algeria
[c] Research Laboratory of Advanced Technology in Mechanical Production, Faculty of Technology, Badji Mokhtar University Annaba, BP.12, Annaba 23000, Algeria
[d] Laboratory of Research on Industrial Risks, Control and Safety, Faculty of Technology, Badji Mokhtar-Annaba University, BP12, Annaba 23000, Algeria
[e] Arts et Metiers Institute of Technology, Université de Lorraine, LCFC, HESAM Université, Metz F-57070, France
[f] Department of Physics, College of Sciences, Taif University, P.O. Box 11099, Taif 21944, Saudi Arabia
[g] Research Unit on Emerging Materials (RUEM), University Ferhat Abbas of Setif 1, Setif 19000, Algeria
[h] Department of Chemistry, Faculty of Sciences, University of M'sila, M'sila 28000, Algeria
[i] Hourani Center for Applied Scientific Research, Al-Ahliyya Amman University, Amman 19328, Jordan
[j] Department of Biosciences, Saveetha School of Engineering, Saveetha Institute of Medical and Technical Sciences, Chennai 602105, India

ARTICLE INFO

Keywords:
FSW
Finite element
FLD
Nakazima
Second derivative

ABSTRACT

The present work involves numerical modeling of the Forming Limit Diagram (FLD) in a heterogeneous weld bead generated by FSW of two aluminum alloys (AA2139-T8 and AA7020-T651) through Nakazima test simulation using Abaqus software and the second derivative of the large deformation criterion to locate the necking. A concept is proposed to determine the FLD of welded bi-material sheet by the extrapolation method and the direct method. In the extrapolation method, FLDs have been predetermined for each of the seven weld zones and extrapolated into FSW configuration. In the direct method, a simplified geometrical model limiting FSW zones is used to determine the FLD for the global FSW bi-material assembled sheet. Results show that the extrapolation method is slightly lower, they agree well with the direct method that shows acceptable values of the major and minor strains, particularly in the expansion region, thus providing good indicative strain values during drawing. The direct method was found to provide a more conservative and realistic prediction of forming limits, especially in strain paths representative of deep-drawing operations, where failure is governed by the material behavior in the expansion region. It was also observed that the heat affected zones govern the onset of localized necking, while the base material AA2139-T8 exhibits the highest formability level among all weld zones. This is the first study to compare two different simulation approaches for FLD extraction in a fully heterogeneous FSW weld bead. The proposed methodology provides a practical numerical framework for predicting the formability of dissimilar aluminum welded sheets and can assist in the design and optimization of lightweight components in the aerospace, automotive, and structural industries.

1. Introduction

In terms of lightweight design, aluminum alloys are proved to be very suitable materials because of their good mechanical properties that are required in aeronautic, aerospace, automotive and defense industries [1,2]. Nowadays, the need to optimize the design of the part with good mechanical properties is strongly required. Therefore, assembling dissimilar aluminum alloy sheets in terms of mechanical and cost properties for example one alloy presenting respectively medium performance alloy with low production cost and the second alloy presenting high performance with high production, obviously contributes to low-cost production of structural components with good mechanical properties [3]. However, as the weld bead is relatively heterogeneous and complex particularly when dissimilar materials are joined, a good understanding of the mechanical properties is first required. Therefore, research workers have concentrated their efforts of the understanding of

* Corresponding author.
E-mail address: m.fatmi@univ-setif.dz (M. Fatmi).

https://doi.org/10.1016/j.mtcomm.2025.114599
Received 4 November 2025; Received in revised form 15 December 2025; Accepted 29 December 2025
Available online 30 December 2025

in one hand the global and local mechanical properties and microstructure and in the other hand the formability of the FSW dissimilar metal sheets and. For instance, Mishra RS and Ma Zy [4] have presented a review article reporting the current state of understanding and development of the FSW and FSP (friction stir processing) particularly on the mechanisms responsible for the formation of welds and microstructural refinement and also on the effects of FSW/FSP parameters on resultant microstructure and final mechanical properties. Lockwood et al. [5] and Lockwood and Reynolds [6] have investigated the global and local mechanical response of heterogeneous structures on the local constituents of the friction stir welded aluminum plates. The viability of modelling and simulation response has been achieved through comparison to experimental results. Liu and Chao [7] have determined global mechanical response of FSW plates by using local constitutive properties on the base metal, heat affected zone and weld nugget and adopting the principle of rule of mixtures to develop analytical models. Moreover, Simar et al. [8] have sorted out the effect of the welding speed on the microstructure; local and overall mechanical properties of friction stir welded joints in the aluminum alloy.

Obviously, in industrial application specifically for most automotive components produced by conventional stamping lines, it is important to know the material formability as each component is geometrically complex and the material blank is usually being subjected to combination of stretching and drawing operations. Therefore, material's forming limit diagram (FLD) is essential in the production of quality stamped product. Most of the research works on FLD deal with single material sheets. Shabadi et al. [9] using FLD have studied the influence of crystallographic texture on room temperature mechanical behaviour of the aluminum alloy AA7020 sheets processed to different thicknesses through rolling. Safdarian et al. [10] have conducted comparative study of FLD prediction of tailor welded blanks in order to determine the performance of numerical approaches such as Müschenborn-Sonne FLD (MSFLD), FLD criterion (FLDcrt) and Ductile Fracture Criterion (DFCcrt), as well as new numerical method of Second Derivative of Thinning (SDT). Shakeri et al. [11] have made evidence that the FLD is dependent upon the material properties such as strain hardening exponent, strain rate sensitivity parameter, anisotropy parameter, grain size as well as strain path. They concluded that the limit strains in the actual strain path, near the punch radius in cup drawing, are lower than those obtained throughout linear path.

Concerning the formability of dissimilar material sheet, Miles et al. [12] have investigated the formability of FSW dissimilar alloys sheets used to fabricate stamped automotive parts and have shown that FSW process has better formability than gas tungsten arc welding process. Genevois et al. [13], on their comparative study on local and global mechanical properties of dissimilar aluminum FSW plates have shown that local tensile data obtained by strain mapping are in good agreement with the curve obtained by micro-tensile tests, therefore they have suggested that the finite element model to predict the overall weld assembly can be safely used. Grujicic et al. [14] have investigated two-level weld material homogenization for efficient computational analysis of welded structures. They used experimental data to construct in one hand the material model for each weld zone and in the hand the material model for the entire weld. Recent numerical investigations have demonstrated that structural configuration and material heterogeneity play a decisive role in mechanical response and damage evolution [15]. In particular, studies on sandwich composite structures have shown that geometrical characteristics such as core topology significantly influence stiffness and strength [15,16]. Advanced finite element formulations recently applied to layered systems further indicate that simplified theories fail to capture transverse shear effects and interlayer stress continuity, highlighting the need for zone-sensitive constitutive descriptions in heterogeneous materials [16].In parallel, numerical studies on cyclic plasticity and ratcheting revealed that loading history, frequency, and hardening parameters strongly affect strain accumulation and instability development, which is directly relevant to forming limit prediction [17]. Recent works on friction stir processing confirmed that numerical simulations can reliably describe strengthening mechanisms while preserving acceptable formability [18]. In addition, studies based on nonlinear and multiphysics formulations demonstrated that combined thermal, magnetic, and mechanical effects significantly influence deformation and stability behavior [19,20]. Finally, investigations in shipbuilding applications showed that friction stir welding can improve strength without compromising formability and that finite element and data-driven methods provide reliable predictions of forming behavior [21].

Recent advances in computational mechanics have highlighted the integration of artificial intelligence with nonlinear numerical modeling. Neural networks and data-driven techniques have been successfully combined with finite element methods to simulate complex systems governed by multiphysics interactions such as heat transfer, dissipation, and external fields [22,23]. In parallel, finite element formulations applied to complex geometries and magnetized flows demonstrated that geometric complexity and external physical effects strongly influence transport behavior and entropy generation, confirming the necessity of advanced nonlinear solvers in engineering applications [24]. Moreover, recent developments in numerical algorithms have focused on high-accuracy time-integration schemes. Exponential integrators and compact finite difference formulations significantly improved numerical stability and convergence in solving nonlinear time-dependent partial differential equations, which is directly relevant for realistic simulation of forming processes and strain localization phenomena [25,26]. Finally, numerical studies on natural convection in complex enclosures confirmed that coupled thermal–geometric effects govern heat dissipation efficiency, further emphasizing the need for robust numerical modeling strategies in systems with strong thermal gradients [27].

In the present study, the aluminum alloys AA2139-T8 and AA7020-T651 were selected due to their complementary properties. The AA2139-T8 alloy, belonging to the Al–Cu–Mg–Ag series, offers high strength and good thermal stability, which makes it suitable for aerospace and defense applications. The AA7020-T651 alloy, from the Al–Zn–Mg family, is relatively less expensive, exhibits good formability, and is widely used in automotive and structural applications. Combining these two alloys in a single structure allows achieving an optimal balance between mechanical performance and production cost. Friction Stir Welding (FSW) was chosen as the joining technique because it enables defect-free solid-state bonding of dissimilar aluminum alloys without melting, thus avoiding issues such as porosity and hot cracking that typically occur in fusion welding. FSW also produces fine-grained microstructures in the stir zone, ensuring superior mechanical integrity and consistent properties across the weld bead. Therefore, FSW provides a reliable approach for joining AA2139-T8 and AA7020-T651 sheets in lightweight structural components. Despite the significant progress in experimental characterization of friction stir welded joints and numerical simulation of forming limit diagrams in homogeneous sheets, a clear gap remains in the literature regarding FLD prediction for fully heterogeneous FSW joints composed of dissimilar aluminum alloys. In particular, no previous study has presented a direct numerical comparison between extrapolated FLD envelopes and a multi-zone direct simulation approach within a unified framework. Therefore, the present work aims to bridge this gap by proposing and comparing two numerical strategies (extrapolation method and direct method) to predict the forming limit behavior of an AA2139–AA7020 FSW joint. From a theoretical perspective, the prediction of strain localization using standard displacement-based finite element formulations is known to involve intrinsic limitations. Classical continuum formulations do not incorporate an internal length scale, which may lead to mesh dependency and an ill-posed description of localization phenomena once material instability or softening develops. These theoretical limitations have been widely discussed in the literature on strain localization and forming limit prediction, particularly in heterogeneous materials such as welded joints. To address these issues, enriched and enhanced finite element

formulations have been proposed, including nonlocal, gradient-enhanced, and embedded discontinuity approaches. The mathematical rationale underlying these formulations lies in the introduction of additional kinematic enrichments or internal length scales, which regularize the localization process and improve the objectivity and accuracy of strain concentration prediction in complex heterogeneous media.

In the present work, standard finite element formulations combined with a Swift hardening law and a second-derivative-based necking criterion are deliberately adopted. The objective is not to develop a new theoretical framework for strain localization, but rather to provide a consistent and controlled numerical setting for comparing two FLD prediction strategies namely, the extrapolation method and the direct heterogeneous modeling approach under identical constitutive and numerical assumptions. This choice allows isolating the influence of material heterogeneity and modeling strategy on FLD prediction while remaining consistent with widely used numerical practices reported in the literature. The aim of the present work is to propose a concept for modeling and determining FLD in a heterogeneous weld bead generated by friction stir welding (FSW) of two aluminum alloys by extrapolation method and direct method. The concept is based on the identification of the materials properties around the weld bead [28], generated by the FSW process, the simulation of the Nakazima test [29]and determining the Localized Necking using the second derivative of the large deformation criterion [30].

2. Methodology of concept

The concept of determining the FLD in FSW bead is presented schematically in Fig. 1, consisting of four main steps. The different friction stir welding zones are clearly identified for both base materials to eliminate any confusion. The advancing side corresponds to the AA2139-T8 alloy, which includes the base material (BM2139), the heat-affected zone (HAZ2139), and the thermo-mechanically affected zone (TMAZ2139). The retreating side corresponds to the AA7020-T651 alloy, which includes the base material (BM7020), the heat-affected zone (HAZ7020), and the thermo-mechanically affected zone (TMAZ7020). The central Nugget (Stir Zone) represents the mixed region where material from both alloys is mechanically intermixed during the FSW process. This schematic ensures that each weld zone is distinctly associated with its corresponding alloy and removes the inconsistency noted in the previous version.

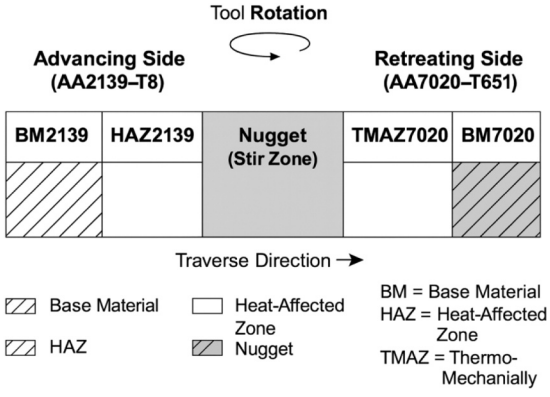

Fig. 1. Schematic illustration of the friction stir welding (FSW) zones in a dissimilar joint between AA2139-T8 (advancing side) and AA7020-T651 (retreating side). The advancing side includes BM2139, HAZ2139, and TMAZ2139; the retreating side includes TMAZ7020, HAZ7020, and BM7020. The central Nugget (Stir Zone) represents the mixed region between both alloys.

2.1. Input data

Must be clearly identified in terms of zoning the FSW bead materials and also their properties. The welding configuration and results considered for the work is published in the work of Bertrand et *al.* [31]. and from the experimental work of Mr. Robe's thesis [28]. It corresponds to a butt weld configuration of an aluminum sheet AA2139-T8, placed on the Advancing Side, and an aluminum sheet AA7020-T651, placed on the Retreating Side. The welded thickness is 5 mm and with a tool placed on the seam. The parameter included in this study concerns one of the extreme points of the operative weldability range. It is a test with the following parameters: feed speed 250 mm/min, rotational speed 600 rpm, tilt angle 2,5°. The tool used has a diameter of 15 mm and a pin length of 4.8 mm. The experimental data of these works [28,31] have been exploited in this article. The tool features a cylindrical shoulder with 15 mm diameter, a pin length of 4.8 mm, and a threaded cylindrical pin profile. In the Nakazima simulations, the punch contacts the AA2139-T8 side (advancing side), which is the stiffer of the two alloys. This choice reflects a conservative forming configuration, likely to localize strain on the stronger side. The FSW process is conducted on two base aluminum alloys AA2139-T8 and AA7020-T651 with the chemical composition given in Table 1.

Then the corresponding geometry of the FSW bead zones generated by the process should be modeled. In fact, when joining two materials through FSW weld, the weld bead is composed of five zones: the nugget when steering two plates, a thermally affected zone for each material and a thermo-mechanically affected zone for each material. Five zones are distinguished, as each zone has different characteristics. For a convenience of the simulation process, the geometrical model of the FSW sheet can be illustrated in Fig. 2, which shows the border of each zone including the two base materials. So, using image processing through Origin Software, a simplified geometrical model is sorted out and consist of seven zones; the base material BM2139-T8, the Base material BM7020-T651, the Nugget, the respective heat affected zone of 2139-T8 and 7020-T651 aluminums, HAZ2139 and HAZ7020, and the respective thermo mechanical affected zones of TMAZ 2139 and TMAZ7020 aluminums. One of the main difficulties is to sort out the tensile properties of the FSW bead zone since tensile specimen cannot be prepared from any zone of the bead. Nevertheless, using Hugo Robe [28–31] experimental data, the tensile properties have been extrapolated and the tensile stress strain curves for the seven zones are plotted. Moreover, due to geometric limitations, precise sampling from narrow zones such as TMAZ or HAZ introduces variability, and these approximations can affect the assigned material behavior. Due to the very limited physical width of the TMAZ and HAZ regions, direct mechanical testing of these zones is experimentally difficult. Therefore, the mechanical properties assigned to these narrow weld regions were reconstructed by extrapolation from strain mapping and inverse identification methodologies reported in the literature by Robe [28] and Bertrand et al. [31]. This introduces uncertainty related to the assumed zone widths, the reconstruction of stress–strain behavior, and the curve fitting procedure using the Swift hardening law. However, since the same material dataset is consistently applied in both the extrapolation and direct FLD approaches, these uncertainties affect both methods similarly and do not alter the comparative conclusions of this study. Future work will focus on experimental characterization and hardness mapping to refine zone-specific properties.

2.2. Analytical calculus

In addition to the main tensile properties, the work hardening law parameters must be computed from the plastic zone of the tensile curve. In the present work, the Swift's law is applied, Eq. (1).

While the Swift law provides a reasonable approximation of work hardening, it does not capture the full complexity of microstructural evolution in welded zones. More advanced constitutive models may be

Table 1
Chemical composition of 2139-T8 and 7020-T651.

Material	Zn	Mg	Fe	Si	Cu	Ag	Cr	Mn	Ti	Ni	Al
2139-T8	0.041	0.43	0.07	0.031	4.92	0.33	0.0022	0.31	0.12	0.005	Bal.
7020-T651	4–5	1–1.4	0.40	0.35	0.2	/	0.1–0.35	0.05–0.5	/	/	Bal.

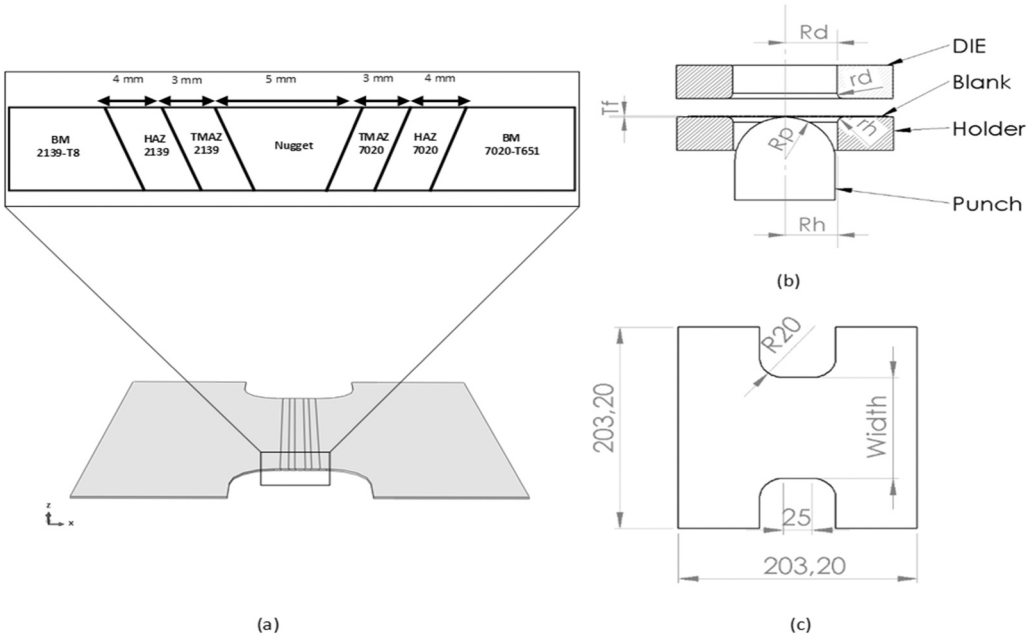

Fig. 2. Nakazima test parts dimensions:(a) Simplified specimen geometrical model describing the seven material zones generated by the FSW joining of two aluminum alloy sheets, (b) Nakazima test: ISO 12004–1, (c) Nakazima specimen blank geometry.

explored in future studies.

$$\overline{\sigma} = K(\varepsilon_0 + \overline{\varepsilon})^n \quad (1)$$

where σ represents the equivalent stress (in MPa), ε represents the equivalent plastic strain (dimensionless), K is the strength coefficient (in MPa), ε_0 is the pre-strain constant (dimensionless), and n is the strain-hardening exponent (dimensionless)for a given material,Once the work hardening law parameters are determined, and then the first thing to achieve before starting the simulations is to simulate the mechanical behaviorof the materials and validatethem through theexperimental tensile curves. It should be noted that the Swift hardening law is adopted in this work as a first-order constitutive approximation to ensure consistency across all weld zones and to isolate the influence of the numerical strategy on FLD prediction. The analytical identification of material parameters from input data obtained from the literature is directly implemented into the finite element simulations, ensuring consistency between constitutive modeling and numerical prediction. Although more advanced constitutive models could describe microstructural effects with greater accuracy, the present objective is a comparative methodological assessment rather than detailed material characterization. Therefore, a common constitutive framework is intentionally applied to all zones to enable a fair comparison between the extrapolation and direct approaches.

2.3. Simulation

The simulations consist in reproducing the Nakazima test according to ISO 12004–1 standard. A blank sheet is blocked between the holder and the die which is pushed by a punching tool until it breaks.The blank sheet can get different initial shape. The main parameters for Nakazima test are given in Table 2 and the Nakazima specimen geometry is shown in Fig. 2c. The principal of Nakazima tests relies of modifying the width of the specimen and observing the behavior of the drawn sheet. The different values of the specimen width are 25.4, 50.8, 101.6, 127, 165.1 and 203.2 mm.

Table 2
Nakazima test parameters (mm).

Parameters	Designation	Values
R^d	Die Internal radius	53
r^d	Die corner radius	6.35
R^h	Blank holder radius	53
r^h	Blank holder corner radius	6.35
R^p	Punch radius	50.8
T(f)	Blank thickness	1

The simulations of Nakazima test are carried out by two type of sheet material properties; homogenous and heterogeneous.

1) In case of homogenous material, a series of sevenNakazima test simulations are conducted on sheets that are characterized by their respective mechanical properties according to material location in the FSW bead zones (BM 2139-T8, BM 7020-T651, HAZ 2139, HAZ 7020, TMAZ 2139, TMAZ 7020, Nugget).
2) In case of heterogeneous material, Nakazima test simulation is applied on the bi-material sheet in which the mechanical properties are attributed respectively to each of the seven corresponding FSW weld zone.

The numerical simulations have been investigated using the finite element software Abaqus. The specimen is modeled with the solid element type Reduced 8-node linear integration (C3D8R).

The boundary conditions in the numerical model is X and Y

symmetry are represented by blocked displacements in the Y and X direction, respectively. The blank partition under blank-holder is blocked in the all directions. The displacement in Z-axis for die and blank-holder is blocked but, for the punch is 30 mm. The coefficient of friction (μ) is defined by $\mu = 0.04$. In each simulation, four steps are illustrated as shown in Fig. 3. A mesh refinement check was performed in the weld bead and expected necking zone by reducing the element size locally. The strain localization patterns and extracted forming limit points showed no significant variation with moderate mesh refinement, indicating that the predicted FLDs are not sensitive to mesh size for the comparative purposes of this study. The strain localization patterns and extracted forming limit points showed no significant variation with moderate mesh refinement, indicating that the predicted FLDs are not sensitive to mesh size for the comparative purposes of this study.A grid sensitivity analysis was conducted using three levels of mesh density, with progressive refinement applied in the weld region and necking area. The differences in predicted forming limit strains between successive mesh refinements were found to be less than 2 %, confirming the mesh-independent nature of the obtained numerical results. Therefore, the intermediate mesh density was selected as a compromise between numerical accuracy and computational efficiency.Numerical convergence was controlled by specifying a residual tolerance of 10^{-4} for all degrees of freedom. Convergence was further verified by monitoring the punch force–displacement response and strain evolution histories to ensure numerical stability across all simulation steps.

2.4. Output

The output presents the results that are allowed to determining the FLD. In the present work two methods have been used. In the first method FLD have been plotted for each bead zonei.e., the material is considered as homogenous in all sheet for each zone properties. The FLD for the whole sheet is extraplatedfrom the seven FLD. In the second method, the FLD is determined for the whole sheet. In this case the geometrical model is divided into seven partitions. So, the material is considered as heterogenous in all sheet, its properties and Swift parameters have been assigned according to each zone. The two formal FLDs have been compared for validation.

3. Results and discussion

3.1. Material properties

Fig. 4 illustrates the tensile curves of each FSW bead zones. Plotting the stress-strain engineering curves reveals that the initial stress and strain of the base materials decrease when the materials are joined by the friction stir welding process. Effectively, AA 2139-T8 material is most resistant and present much strain, meanwhile AA 7020-T651 is about 20 % less resistant and 25 % less strained. The tensile properties for the bead zones show significant decrease. The elastic stress dropped by 45–55 % relatively to the value of elastic stress of AA 2139-T8. The ultimate stress shows practically the same value of 376 MPa which is about 30 % lower than the ultimate stress of AA 2139-T8. However, the values of the strain are quite fluctuating from 0.21 % to 8.56 %. That is quite difficult to check unless tensile tests are carried out for specimens prepared from each bead zone. Nevertheless, in the present work the values of the strains for each bead zone are adopted. The corresponding mechanical properties are determined and presented in Table 3. Note

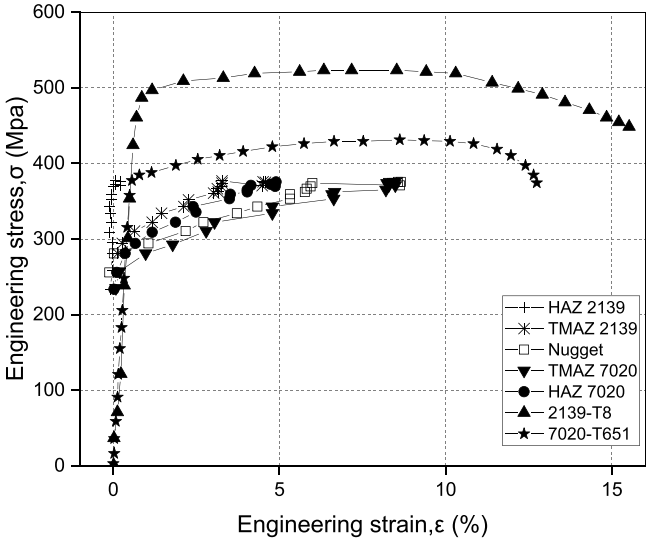

Fig. 4. Tensile curves of materials around the FSW bead.

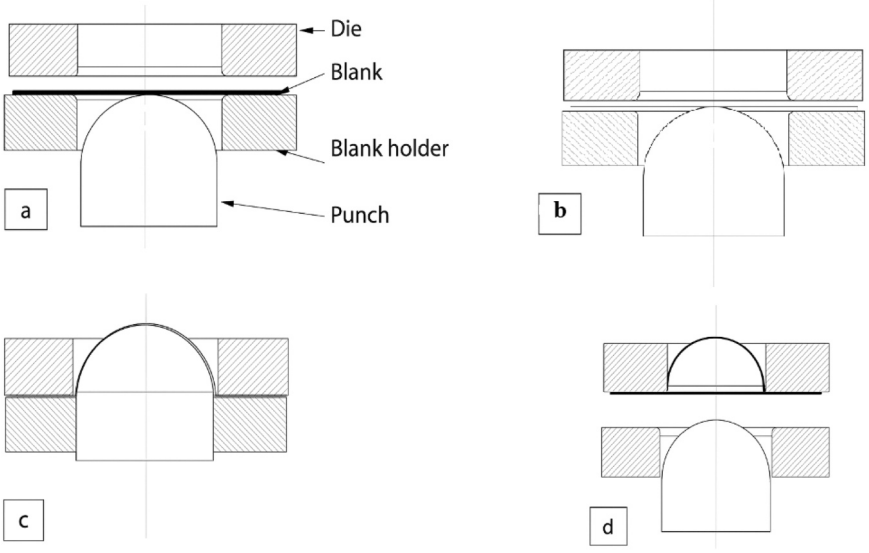

Fig. 3. Nakazima test simulation steps: **a)** Blank placement on the die,**b)** blank clamping and punch placement,**c)** deep drawing,**d)** end of operation and deep-drawn part ejection.

Table 3
Mechanical properties around FSW sheet bead made of 2139-T8 and 7020-T651.

	BM 2139-T8	HAZ 2139	TMAZ 2139	Nugget	TMAZ 7020	HAZ 7020	BM 7020-T651
σ_y(MPA)	505	234	280	256	234	235	395
σ_u(MPA)	529	376	376	375	375	375	445
A(%)	15.6	0.21	4.57	8.56	8.48	4.86	11.5

BM: Base material; HAZ: Heat Affected Zone; TMAZ: Thermo-mechanical Affected Zone

that engineering stress-strain curves are shown for illustrative purposes, while true stress-strain data were used in the finite element simulations and Swift law fitting.

3.2. Swift law parameters

Using Swift's law Eq. (1), the values of *K* and *n* for the seven FSW bead zones are given in Table 4. The values of *K*and *n* are respectively 725 MPa and 0.12 in the base material 2139-T8 and 645 MPa and 0.1 in the basematerial7020-T651 there is respectively a difference of 10 % in the value *K* and 15 % in the value of *n*. After friction stir welding, the behavior of the creep region in the bead weld zones has changed showing a decrease of the value *K* by 45–30 % relatively to the mean value of the two base materials. Similar observation is found for the values of*n*. However, for the HAZ 2139 zone, the values of *K*and *n*are quite low and should be checked. Nevertheless, within the present work these values of *K* and *n* have been adopted in the simulation investigation.

3.3. Nakazima simulation results

Simulation of Nakazima test consists in applying a drawing operation according to the steps described in Section 2.1. Numerical results are illustrated in Fig. 5a; showing the strain distribution where a critical zone is made in which the maximum strain occurs corresponding to the undesirable Localized Necking. The drawing progression generates strains that are recorded as a function of time along the whole drawing process. Once the simulation of the Nakazima test is finished then the second derivative of major strain over the time of the whole drawing process is obtained for its maximum value (Fig. 5b). The method of determining the second derivative of major strain is well explained in literature 30 [17]. The major strain corresponds respectively to the values of the reached strains at the time where the second derivative of the major strains is higher. The same method was used to determine the minor strain.The second derivative of major strain was selected as the necking detection criterion because it provides a localized and objective indication of strain instability during forming. Unlike empirical criteria such as FLD or Müschenborn–Sonne, the second derivative method directly identifies the onset of strain localization from the numerical response without requiring calibration parameters. It has been successfully applied in several recent numerical and experimental investigations on forming limit prediction, including Heidari et al. [30] and Lumelskyj et al. [29], where its robustness in detecting localized necking was demonstrated. Therefore, the use of the second derivative criterion in this study is well supported by the literature.

Table 4
Swift parameters K & n for FSW zones of two aluminum alloys.

FSW zone	MB 2139-T8	HAZ 2139	TMAZ 2139	Nugget	TMAZ 7020	HAZ 7020	MB 7020-T651
K(MPa)	725	391	455	491	481	479	645
n	0.12	0.04	0.06	0.09	0.09	0.08	0.1

3.4. FLD determination

Strain values (major and minor) were extracted from FE simulations by tracking principal in-plane strains at the integration points near the necking zone. These strains were averaged across a small region to reduce noise.In the present work, The FLD have been determined through simulation of Nakazima test. The FLD is quite complex to simulate because when stir welding two sheets of two types of aluminums the weld bead is submitted to metallurgical transformation generating heat affected zones and thermo-mechanical-affected zones. Then two methods for determining the FLD are suggested. In the first method FLD is plotted for each bead zone. So, from the seven FLD, the FLD for the whole sheet is extrapolated considered here as the extrapolating FLD method. In the second method, the FLD is determined for the whole sheet considered as the direct FLD method. In this case the geometrical model for these simulations process is divided into seven partitions that are characterized by their mechanical properties. The material properties and Swift parameters have been assigned according to each zone. The two formal FLD are then compared for validation.The differences in formability observed between the weld zones can be physically attributed to the microstructural heterogeneity induced by the friction stir welding process. The base material AA2139-T8 exhibits the highest forming limits due to its higher strain hardening capability, whereas the HAZ zones show reduced limits as a result of thermal softening and microstructural coarsening. The nugget and TMAZ regions present intermediate behavior, reflecting the combined effects of dynamic recrystallization and partial retention of parent material properties.Furthermore, a clear methodological distinction is observed between the extrapolation and direct approaches. The extrapolation method defines upper and lower bounds based on zone-wise FLDs, providing an envelope of possible forming limits. In contrast, the direct method accounts for strain redistribution across the entire welded sheet within a unified finite element model, leading to a more realistic description of the local strain paths and interaction between zones. This explains why the direct FLD tends to be more conservative in the expansion region, where strain localization is governed by the weakest weld zone.

3.4.1. Extrapolating FLD method

The respective minor and major strains for the Nugget, Heat Affected Zone, and thermo-mechanical-affected zone for both materials generated by the FSW process. The FLD of the base materials are quite distinguishable according to the major and minor strains (Fig. 6). Then when approaching the weld bead, the FLD are disturbed and the new forming limits can be fitted within the two base materials FLD. In the expansion region, when the minor strain is greater than 0, the FLD for the base material 2139-T8 is the highest which is obvious as the BM 2139-T8 material presents higher materials properties and Swift's parameters. However, the FLD for HAZ 2139 zone is the lowest. The FLD for the other zones (BM7020-T651, Nugget, TMAZ 7020, HAZ 7020 and TMAZ 2139) are situated within the higher and the lower FLD corresponding to respectively the BM 2139-T8 and HAZ 2139. In the negative minor strain region, when the minor strain is less than 0, the FLD for the base material 2139-T8 can be considered as the lowest and the FLD of the HAZ 7020 as the highest value. The FLD of the other bead zones can be fitted within the higher and the lower FLDs. As a consequence, the FLD for the whole bi-material sheet composed of two aluminum sheets (2139-T8 and 7020-T651 materials) can be extrapolated from the above FLDs for the Nugget, Heat Affected Zone and thermo-mechanical-affected zone for both materials. The idea is the reconstruct is to fit the seven FLDs within the higher limit and the lower limit in both regions respectively the expansion and negative minor strain region. Hence, the minor and major strains for the FSW bi-material sheet can be illustrated as shown in (Fig. 7). The upper and lower limits in Fig. 7 were obtained as envelopes of the seven zone-based FLDs shown in Fig. 6 using binning of the minor strain domain.Then in both expansion and

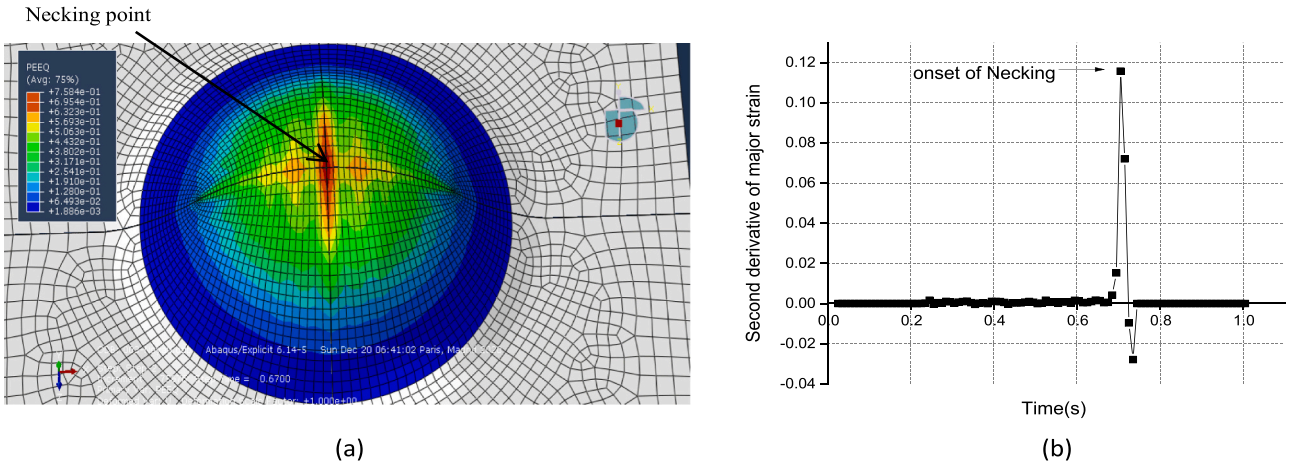

Fig. 5. Strain distribution generated from Nakazima test simulation: a) Necking point area, b) Diagram of the second derivative of major large strain over time The second derivative of strain helps in identifying the onset of localized necking, as described in [30].

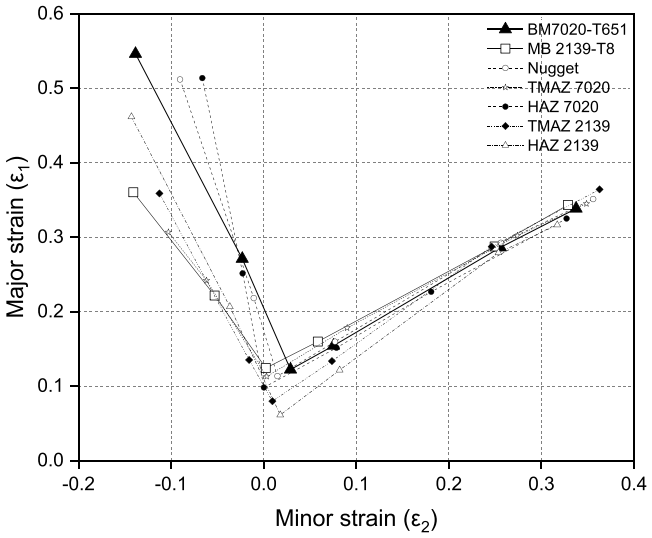

Fig. 6. FLD for seven zones generated by FSW process of two aluminum sheets.

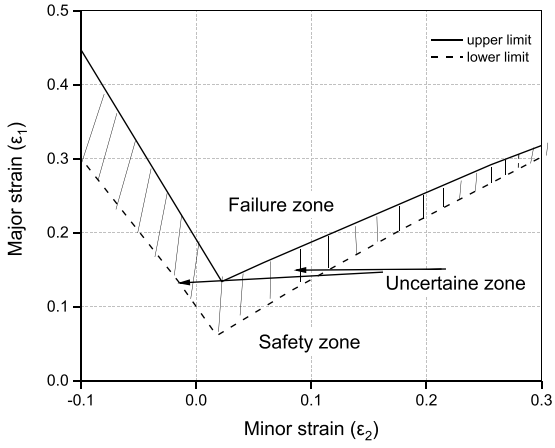

Fig. 7. FLD for a bi-material sheet joined by FSW process obtained by extrapolation method.

negative minor strain region, the FLDs are located within two limits the upper and lower. The former FLD is then characterized by three FLD zones, the failure zone, above the upper limit, the safety zone below the lower limit and the an uncertain zone between the upper and lower limits.

3.4.2. *Direct FLD method*

The direct method consists in simulating the FLD for the bi-material sheet by respecting the respective material properties and Swift's parameters for each zone generated by the FSW process, the geometrical model shown in Fig. 8. In this case, the FLD of the bi-material is illustrated in Fig. 8 showing the minor and major strains that are characterized by conventional limiting lines within the expansion and the negative minor strain region. Conventionally above these lines, the zone is in failure, and below these lines, the zone is safe. It is interesting to note that a few minor strains in the negative minor strain region have resulted from the simulation up to 0.1 of the major strain whereas in the expansion region values of minor strains ranged from −0.02–0.31.A sensitivity analysis was conducted to evaluate the influence of zone width on the FLD predicted by the direct method. The nominal widths of the TMAZ and HAZ regions were varied by ±10 % while keeping the mechanical properties unchanged. The resulting FLDs showed only minor variations in both major and minor strain limits, particularly in the expansion region, confirming that the predicted FLD is not highly sensitive to moderate changes in zone width. This indicates that the

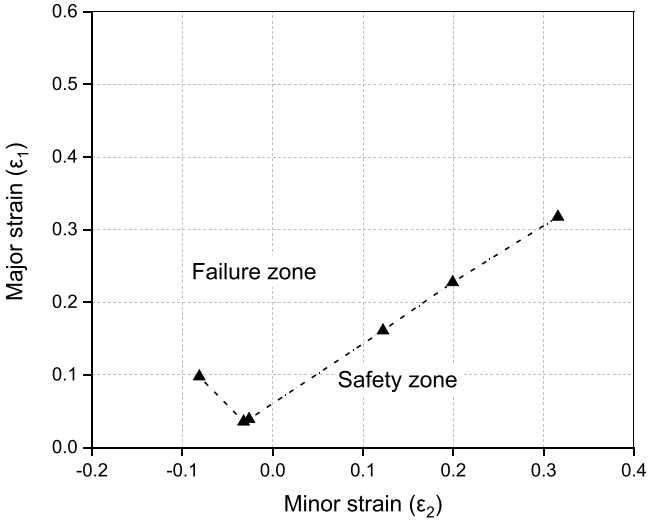

Fig. 8. FLD for a bi-material sheet joined by FSW process obtained by direct method.

simplified geometric representation adopted in this study is sufficient for comparative purposes.

3.5. Validation of the simulation results of FLD for FSW bi-material sheet

It should be noted that no experimental FLD measurements were performed in this study. This is a limitation, and future work will aim to validate the numerical results using physical Nakazima tests and hardness profiles across the weld bead.The simulated results of FLD for FSW bi-material sheet from the extrapolation and the direct methods are fairly interesting as they are in good agreement (Fig. 9). In the expansion region, the FLD given by the direct method is almost the same limit as the lower limit given by the extrapolation method. In addition, the direct method is more representative as the values of the minor strains starts from negative values (0.03) to positive values 0.33. In the negative minor strain region, the direct method resulted in a limit that is lower than the one given by the extrapolation method. Nevertheless, the latter is not that influencing since for deep drawing process, only the expansion region is determinant for conducting safe drawing. Hence in the expansion region, the safety zone can be attributed to the zone below the line given by the direct method. The validation of the proposed numerical model was performed by comparing the predicted strain distribution and the computed forming limit diagram (FLD) with the corresponding results reported by Bertrand et al. [31] and Robe [28]. The comparison showed good agreement in terms of strain localization and limit strain levels, confirming the adequacy and consistency of the proposed modeling concept. The model therefore provides a reliable approach for predicting the formability behavior of the friction stir welded (FSW) dissimilar aluminum sheets AA2139-T8 and AA7020-T651. A qualitative validation was performed by comparing the predicted strain localization patterns and forming limit trends with those reported by Bertrand et al. [31] and Robe [28]. Although experimental FLD curves for the exact AA2139–AA7020 configuration are not available in these references, similar localization modes and relative formability levels were observed. In particular, the location of maximum strain near the nugget and TMAZ regions and the reduced formability in the HAZ zones are consistent with reported findings. This qualitative agreement supports the reliability of the present numerical approach.

4. Conclusion

The present work is a contribution in determining FLDs in heterogeneous weld bead generated by friction stir welding of two aluminum alloy sheet. The investigation relies of the simulation of Nakazima test and determining the Localized Necking using the second derivative of the large deformation criterion. Firstly, a concept of determining the FLD in FSW bead based on four main steps is presented. The first step identifies the input data, the second step completes the first step by the determination of the work hardening parameters, the third step is the Nakazima tests simulation in order to obtain the major and minor strains using the second derivative of the large deformation criterion, and the FLDs are plotted in the final step. Secondly, a simplified geometrical model limiting the FSW zones of the weld bead has been proposed on the bases on Hugo Robe's literature experimental data characterizing the material properties of each zone known as Nugget, Heat Affected Zone and thermo-mechanical-affected zone for both materials. Thirdly, two methods respectively referred as extrapolation method and direct method have been adopted for simulating Nakazima test under Abaqus software to sort out the FLD. In the first method, FLD has been extrapolated from pre-determined FLD of each of the seven weld zones. In the direct method, the FLDs have been determining for the global weld bead with respect to the mechanical properties of each zone of the weld bead. The originality of this study lies in applying a dual-method approach (extrapolation and direct modeling) to derive forming limit diagrams from zone-specific mechanical data. Results show that Nakazima test simulations permit to identify the FLD when using the extrapolation method, obviously for each of the nugget, heat affected zones and thermo-mechanical-affected zones for both materials generated by the FSW process in the bi material sheet. However, the seven FLDs are located between two limiting lines the upper FLD and the lower FLD. Therefore, the extrapolation method suggests FLDs showing a safety zone, a failure zone and an uncertain zone. When using the direct method, the FLD is fairly representative comparing to results of the extrapolation method. It is interesting to find out that in the expansion region, the FLD given by the direct method is in good agreement with the lower FLD given by the extrapolation method. In the negative minor strain region, the direct method resulted in a limit that is too lower to that given by the extrapolation method.Nevertheless, the latter is not that influencing since for deep drawing process, only the expansion region is determinant for conducting safe drawing. Hence in the expansion region, the safety zone can be attributed to the zone below the line given by the direct method.It should be noted that the present work is based on standard finite element formulations. Although advanced enrichment strategies have been reported in the literature to improve strain localization prediction in highly heterogeneous media, their application was beyond the scope of this comparative study. Since the objective was to assess the relative performance of extrapolation and direct FLD approaches under identical numerical conditions, conventional elements were considered sufficient. The use of enriched formulations will be addressed in future investigations to further enhance prediction accuracy in complex welded structures.

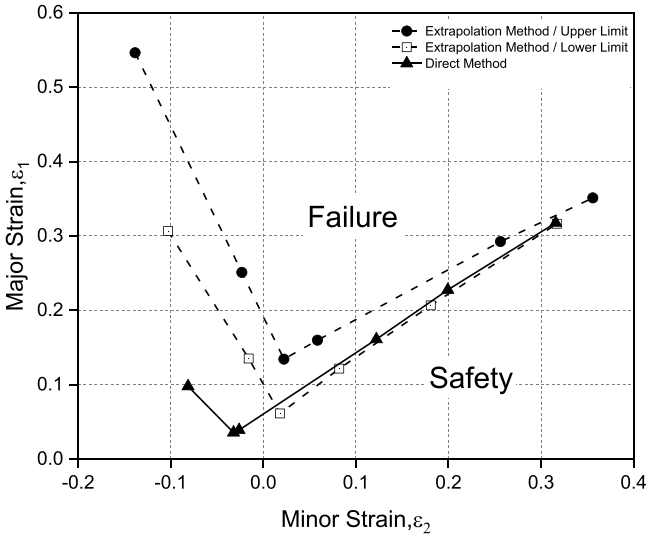

Fig. 9. Comparison of FLD for a bi-material sheet joined by FSW process between extrapolation and direct methods.

CRediT authorship contribution statement

W. Ghennai: Data curation. **Sandra Zimmer-Chevret:** Data curation. **Mohamed Lamine Kheroufi:** Conceptualization. **A. Amirat:** Data curation. **R. Yekhlef:** Conceptualization. **S. Alomairy:** Conceptualization. **D. Belfenneche:** Data curation. **Fatmi M:** Validation. **M.A. Ghebouli:** Data curation. **Aseel Smerat:** Formal analysis.

Declaration of Competing Interest

The authors declare that they have NO conflict of interest.

Acknowledgement

The authors extend their appreciation to Taif University, Saudi Arabia, for supporting this work through project number (TU-DSPP-2024–63).

Appendix A. Supporting information

Supplementary data associated with this article can be found in the online version at doi:10.1016/j.mtcomm.2025.114599.

Data availability

No data was used for the research described in the article.

References

[1] A.K. Jha, P.R. Narayanan, V. Diwakar, K.S. Kumar, M.C. Mittal, Metallurgical analysis of cracked aluminum alloy (AFNOR 7020) components used in satellite launch vehicles, Eng. Fail. Anal. 11 (2004) (2004) 463–474, https://doi.org/10.1016/j.engfailanal.2003.05.016.

[2] M. Kumar, N. Sotirov, C.M. Chimani, Investigations on warm forming of AW7020-T6 alloy sheet, J. Mater. Process. Technol. 214 (2014) 1769–1776, https://doi.org/10.1016/j.jmatprotec.2014.03.024.

[3] Rémi Bertrand, Hugo Robe, Damien Texier, Yasser Zedan, Eric Feulvarch, et al., Analysis of AA2XXX/AA7XXX friction stir welds, J. Mater. Process. Technol. 271 (2019) 312–324, https://doi.org/10.1016/j.jmatprotec.2019.03.027. Elsevier.

[4] R.S. Mishra, Z.Y. Ma, Friction stir welding and processing, Mater. Sci. Eng. 50 (1-2) (2005) 1–78, https://doi.org/10.1016/j.mser.2005.07.001.

[5] W. Lockwood, B. Tomaz, A.P. Reynolds, Mechanical response of friction stir welded AA2024: experiment and modeling, Mater. Sci. Eng. A 323 (1-2) (2002) 348–353, https://doi.org/10.1016/S0921-5093(01)01385-5.

[6] W. Lockwood, A.P. Reynolds, Simulation of the global response of a friction stir weld using local constitutive behavior, Mater. Sci. Eng. A 339 (1-2) (2003) 35–42, https://doi.org/10.1016/S0921-5093(02)00116-8.

[7] S. Liu, Y.J. Chao, Determination of global mechanical response of friction stir welded plates using local constitutive properties, Model. Simul. Mater. Sci. Eng. 13 (1) (2005), https://doi.org/10.1088/0965-0393/13/1/001.

[8] A. Simar, Y. Brechet, B. de Meester, DenquinA, T. Pardoen, Microstructure, local and global mechanical properties of friction stir welds in aluminum alloy 6005A-T6.Materials, Sci. Eng. A 486 (1-2) (2008) 85–95, https://doi.org/10.1016/j.msea.2007.08.041.

[9] R. Shabadi, S. Suwas, S. Kumar, H.J. Roven, E.S. Dwarkadasa, Texture and formability studies on AA7020 Al alloy sheets, Mater. Sci. Eng. A 558 (2012) 439–445, https://doi.org/10.1016/j.msea.2012.08.024.

[10] R. Safdarian, R.M. Natal Jorge, D.Santos Abel, Naeini H. Moslemi, M.P.L. Parente, A comparative study of forming limit diagram prediction of tailor welded blanks, Int. J. Mater. Form. 8 (2015) 293–304, https://doi.org/10.1007/s12289-014-1168-9.

[11] M. Shakeri, B.M. Dariani, A. Sadough, Forming limit diagram of metal sheet in actual strain path with respect to forming process, Trans. Eng. Sci. 32 (9) (2001), https://doi.org/10.2495/CON010141.

[12] M.P. Miles, D.W. Melton, T.W. Nelson, Formability of friction-stir-welded dissimilar aluminum alloy sheets, Metall. Mater. Trans. A 36 (2005) 3335–3342, https://doi.org/10.1007/s11661-005-0008-4.

[13] G. Genevois, A. Deschamps, P. Vacher, Comparative study on local and global mechanical properties of 2024 T351, 2024 T6 and 5251 O friction stir welds, Mater. Sci. Eng. A 415 (1-2) (2006) 162–170, https://doi.org/10.1016/j.msea.2005.09.032.

[14] M. Grujicic, G. Arakere, A. Hariharan, B. Pandurangan, Two-level weld-material homogenization for efficient computational analysis of welded structure blast survivability, J. Mater. Eng. Perform. 21 (2012) 786–796, https://doi.org/10.1007/s11665-011-9876-5.

[15] Habib Achache, Ghezail Abdi, Zagane Mohammed El Sallah, Murat Yaylaci, Rachid Boughedaoui, Sevval Ozturk, Ecren Uzun Yaylaci, Mehmet Emin Ozdemir, Numerical analysis of three-point bending of sandwich panels with different core cross-sections: Finite element study, Adv. Nano Res. 18 (5) (2025) 481–488, https://doi.org/10.12989/anr.2025.18.5.481.

[16] M. Lezgy-Nazargah, Murat Yaylacı, H. Shad, Double superposition shear deformation theory for buckling analysis of layered composite circular closed cylindrical shells in underwater environments, Ocean Eng. 340 (1) (2025) 122230, https://doi.org/10.1016/j.oceaneng.2025.122230.

[17] Sk Tahmid Muhatashin Fuyad, Md. Abdullah Al Bari, Md Makfidunnabi, H.M. Zulqar Nain, Mehmet Emin Özdemir, Murat Yaylaci, Finite element analysis of ratcheting on beam under bending-bending loading conditions, Struct. Eng. Mech. 89 (1) (2024), https://doi.org/10.12989/sem.2024.89.1.023.

[18] Dursun Murat Sekban, EcrenUzunYaylacı, Mehmet Emin Özdemir, Şevval Öztürk, Murat Yaylacı, Subrata Kumar Panda, Formability behavior of AH-32 shipbuilding steel strengthened by friction stir process, Theor. Appl. Fract. Mech. 132 (2024) 104485, https://doi.org/10.1016/j.tafmec.2024.104485.

[19] Rajendran Selvamani, Prabhakaran Thangamuni, Murat Yaylacı, Mehmet Emin Özdemir, Ecren Uzun Yaylacı, Nonlinear vibration and parametric excitation of magneto-thermo elastic embedded nanobeam using homotopy perturbation technique, ZAMM - J. Appl. Math. Mech. 104 (12) (2024) e202400525, https://doi.org/10.1002/zamm.202400525.

[20] R. Selvamani, F. Ebrahimi, M. Yaylacı, et al., Nonlinear poro-thermo-forced vibration in curved sandwich magneto-electro-elastic shells under hygrothermal environment, Acta Mech. 235 (2024) 5489–5528, https://doi.org/10.1007/s00707-024-03994-z.

[21] Dursun Murat Sekban, EcrenUzun Yaylaci, Mehmet EminÖzdemir, Murat Yaylaci, Determination of formability behavior of steel used in ships by various methods, Struct. Eng. Mech. 92 (2) (2024) *89–196*, https://doi.org/10.12989/sem.2024.92.2.189.

[22] Fatima Shafiq Hira, QammarRubbab, Irshad Ahmad, Afraz Hussain Majeed, Advanced computational modeling of Darcy-Forchheimer effects and nanoparticle-enhanced blood flow in stenosed arteries, Eng. Appl. Artif. Intell. 152 (2025) 110737.

[23] Bilal Ahmed, Dong Liu, BouthainaDammak, Naeem Ullah, Afraz Hussain Majeed, Hafedh Mahmoud Zayani, Binjuan Zhao, Artificial intelligence-based multi-expression programming prediction of magnetized radiative nanofluid flow between coaxial deformable tubes, Case Stud. Therm. Eng. 74 (2025) 106825.

[24] Afraz Hussain Majeed, Rashid Mahmood, Dong Liu, Shahid Ullah, Numerical simulations of entropy generation and thermal fluid flow in a wavy enclosure: a NEWTON-PARDISO solver-based study, Int. Commun. Heat. Mass Transf. 162 (2025) 108569.

[25] Y. Nawaz, A.H. Majeed, M. Bin-Asfour, et al., Stability and convergence analysis for coupling of exponential integrator and Runge–Kutta method for eyring-powell fluid under unsteady Electro-Osmosis flow effects, Ricerche mat (2025), https://doi.org/10.1007/s11587-025-00991-9.

[26] Yuyuan Sun, Chenchen Xi, Dong Liu, Miguel Vivas-Cortez, Afraz Hussain Majeed, Muhammad Abbas, Multi-objective optimization of hot water circulation pump using machine learning model and non-dominated sorting genetic algorithm, AIP Adv. 15 (2025) 115301, https://doi.org/10.1063/5.0292666.

[27] S. Ullah, G. Saddiq, A.H. Majeed, I. Alazman, Conjugated heat transfer of entropy generation and hybrid nanoparticles in a cavity, Int. J. Numer. Methods Heat. Fluid Flow. 35 (11) (2025) 4224–4247, https://doi.org/10.1108/HFF-04-2025-0229.

[28] Robe, H.. Apports à la compréhension du soudage FSW hétérogène d'alliages d'aluminium par une approche expérimentale et numérique, (2017) (Doctoral dissertation, Université de Lyon).

[29] Dmytro Lumelskyj, Jerzy Rojek, Dorel Banabic, Lucian Lazarescu, Detection of strain localization in Nakazima formability test experimental research and numerical simulation, Procedia Eng. 183 (2017) 89–94, https://doi.org/10.1016/j.proeng.2017.04.016.

[30] Alireza Heidari, Aazam Ghassemi, Amir Atrian, Numerical and experimental investigation of forming limit diagrams of 6063 aluminum alloy sheets using Ayada ductile fracture criterion and the second derivative of large strain criterion at increased temperature, Lat. Am. J. Solids Struct. 15 (9) (2018) 2018, https://doi.org/10.1590/1679-78254974.

[31] R. Bertrand, H. Robe, D. Texier, Y. Zedan, E. Feulvarch, P. Bocher, Analysis of AA2XXX/AA7XXX friction stir welds, J. Mater. Process. Technol. 271 (2019) (2019) 312–324, https://doi.org/10.1016/j.jmatprotec.2019.03.027.